Available online at www.sciencedirect.com

ScienceDirect

International Journal of Solids and Structures 44 (2007) 8517–8531

INTERNATIONAL JOURNAL OF SOLIDS AND STRUCTURES

www.elsevier.com/locate/ijsolstr

BEM for transient 2D elastodynamics using multiquadric functions

Morcos F. Samaan [a], Youssef F. Rashed [b,*,1]

[a] *Civil Engineering Department, The Higher Technological Institute, Ramadan 10th city, Egypt*
[b] *Department of Structural Engineering, Cairo University, Giza, Egypt*

Received 3 December 2006; received in revised form 26 April 2007; accepted 25 June 2007
Available online 29 June 2007

Abstract

A new boundary element model for transient dynamic analysis of 2D structures is presented. The dual reciprocity method (DRM) is reformulated for the 2D elastodynamics by using the multiquadric radial basis functions (MQ). The required kernels for displacement and traction particular solutions are derived. Some terms of these kernels are found to be singular; therefore, a new smoothing technique is proposed to solve this problem. Hence, the limiting values of relevant kernels are computed. The validity and strength of the proposed formulation are demonstrated throughout several numerical applications. It is proven from the results that the present formulation is more stable than the traditional DRM, which uses the conical $(1 + R)$ function, especially in predicting results in the far time zone.

Keywords: Multiquadric radial basis functions; Boundary element method; Dual reciprocity method; 2D elastodynamics; Transient problem

1. Introduction

Structural dynamic analysis is one of the main required tasks for an engineer to accomplish in the analysis of buildings. Many numerical methods are available in this field such as the finite element method (FEM), (Bathe, 1982), which has some disadvantages such as: the need for discretizing the entire problem domain, and the inaccuracies found in cases of stress concentration. The boundary element method (BEM), (Brebbia et al., 1984), has been used to overcome these problems since it only requires the discretization of the boundary and produces excellent results for stress concentration cases. BEM can also offer easy solution for complex structures in less time and high accuracy.

There are many BEM formulations for treating structures under dynamic loading (Dominguez, 1993). These formulations include the time domain, the Laplace transform, and the domain integral techniques. The main problems of these formulations are the mathematical complications found in the first two and due to the required

* Corresponding author. Tel.: +20 105112949; fax: +20 26875889.
E-mail address: YRashed@bue.edu.eg (Y.F. Rashed).
[1] On leave to The British University in Egypt, El-Sherouk City, Postal No. 11837, P.O. Box 43, Egypt.

0020-7683/$ - see front matter
doi:10.1016/j.ijsolstr.2007.06.023

domain integrations in the last one. To overcome these drawbacks, Nardini and Brebbia (1982) developed a new formulation, which is named later the dual reciprocity method (DRM). In the DRM, the integral equation of the body is presented in terms of its boundary variables and includes a domain integral corresponding to the body inertia forces. This integral can be transformed to the boundary (i.e. excluding the domain terms from calculations) using a new collocation scheme to approximate the field accelerations, or consequently the field displacements. Nardini and Brebbia (1982) suggested the conical $(1 + R)$ function to be used in this approximation. After that, the DRM has been used to solve various types of differential equation problems including potential, fluid dynamics, and heat transfer problems (Partridge et al., 1992). The using of DRM in solving elastodynamics is reported in few publications (for more details, see Dominguez, 1993). Among these publications is the work of Bridges and Wrobel (1994) where spline functions are used in modeling structural free vibrations. Rashed (2002a) used the Gaussian function to solve transient problem then he extended his formulation to the compact support functions (Rashed, 2002b). The nonlinear applications are also studied in the works of Kontoni and Beskos (1993), Telles and Carrer (1994), and Coda and Venturini (2000). Perez-Gavilan and Aliabadi (2000) extended the DRM to Galerkin-type collocation method.

The choice of suitable approximation function is very important in the DRM formulation since it directly affects the result accuracy. Among all proposed function, is the conical $(1 + R)$ function, which is commonly used in many applications. According to Golberg and Chen (1994), this function is just one from a class of functions called the radial basis functions (RBFs). The thin plate spline function (TPS) is another function which was chosen by other researchers. In their applications, Bridges and Wrobel (1994), Golberg (1995), Chen (1995), and Karur and Ramachandran (1995) concluded that the TPS function had much improved the results accuracy. But, in contradiction to this conclusion, Agnantiaris et al. (1996) compared the behavior of polynomial RBFs against thin plate splines ($R^2 \ln R$) for 2D elastodynamics. They (Agnantiaris et al., 1996) concluded that the conical $(1 + R)$ function produces the best numerical results. Therefore, such function is implemented inside the commercial software package—BEASY (Niku and Adey, 1996). Several studies were carried out in order to rank the radial basis functions according to their best interpolation of multivariate data or functions. An interesting study in this field was introduced by Franke (1982) who reviewed all available radial basis functions for interpolating scattered data sets. Among the tested functions, Multiquadrics (MQ), $(R^2 + C^2)^{1/2}$ (Hardy, 1971; Hardy, 1990, and Wendland, 2002), were ranked the best in accuracy, followed by Duchon's thin plate splines (TPS). The reason for considering the MQ function to be the best in interpolations is for its exponential convergence rate (Powell, 1994), whereas this rate is just linear in the case of the TPS function (Madych and Nelson, 1992).

The use of the MQ function within the context of the DRM can be summarized as follows: Golberg et al. (1996) utilized the MQ function in approximating the forcing term of Poisson's differential equation to be able to solve potential problems in Laplacian form. They concluded that the obtained results using the MQ interpolation are highly accurate. Later, Agnantiaris et al. (2001) used the MQ function to investigate the behavior of 3D non-axisymmetric and axisymmetric structures under the effect of free vibrations. However, the application of MQ function in 2D elastodynamics has never been reported previously.

In this paper, the application of the DRM in dynamic analysis of 2D elastic structures is formulated using the MQ radial basis functions. The dynamic problem is analyzed by considering first the homogeneous equation (the static case) to be solved using the well-known static fundamental solution as a complementary one. The non-homogeneous state (the dynamic case) is solved using a particular solution developed from a MQ collocation scheme. The expressions for displacement and traction particular solutions for the MQ interpolation are derived. A smoothing technique is introduced in order to solve the singularity problem appeared in some terms of the formerly derived expressions. This treatment leads to final smooth forms of displacement and traction particular solutions, which will be used in the calculations in this paper. The limiting case (as $R \to 0$) is studied and the values of particular solutions at this case are obtained in explicit form. Finally, several numerical problems are studied to demonstrate the validity and accuracy of the proposed formulation.

2. Integral equations of 2D elastodynamics

Consider the 2D structure shown in Fig. 1 with domain Ω and boundary Γ is being under general dynamic loading. The equilibrium equations at a general point x on this body in terms of displacements (Navier's equations), and in absence of body forces, are given by (Brebbia et al., 1984):

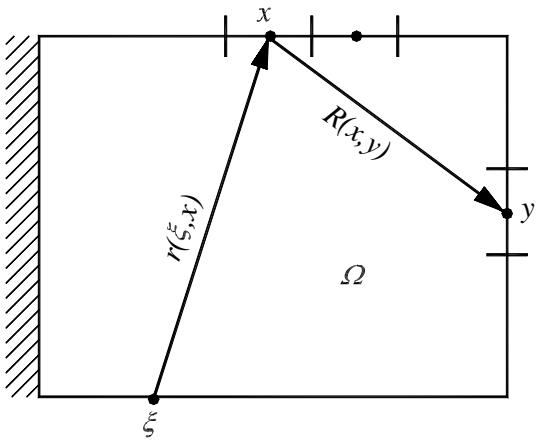

Fig. 1. Body geometry and boundaries.

$$Gu_{i,jj}(x) + \frac{G}{(1-2v)}u_{j,ji}(x) = \rho\ddot{u}_i(x) \tag{1}$$

where the tensor (indicial) notation is used; the comma denotes derivatives with respect to spatial coordinates, and the index repetition means summation G is the shear modulus, v is the Poisson's ration, ρ is the mass density, and $\ddot{u}_i(x)$ is the acceleration at the point x (the over dots denotes derivatives with respect to time).

Consider the displacement solution of Eq. (1) to be divided into two parts; the complementary part $u_i^c(x)$, and the particular part $u_i^p(x)$. The complementary solution, $u_i^c(x)$, is the solution of the homogeneous part of Eq. (1) that satisfies the body boundary conditions. The particular solution, $u_i^p(x)$, on the other hand, is the solution that satisfies the non-homogeneous part of Eq. (1) with no boundary conditions. Applying the concept of the DRM (Nardini and Brebbia, 1982), the final integral representation can be obtained as follows:

$$c_{ij}(\xi)u_j(\xi) + \int_{\Gamma(x)} T_{ij}(\xi,x)u_j(x)\,\mathrm{d}\Gamma(x) = \int_{\Gamma(x)} U_{ij}(\xi,x)t_j(x)\,\mathrm{d}\Gamma(x) + \left[c_{ij}(\xi)u_j^p(\xi) + \int_{\Gamma(x)} T_{ij}(\xi,x)u_j^p(x)\,\mathrm{d}\Gamma(x) - \int_{\Gamma(x)} U_{ij}(\xi,x)t_j^p(x)\,\mathrm{d}\Gamma(x)\right] \tag{2}$$

where ξ is a source point, x is a field point, and $c_{ij}(\xi)$ is the jump term; $c_{ij}(\xi) = \delta_{ij}/2$ if $\xi \in \Gamma$ (smooth boundary), and $c_{ij}(\xi) = \delta_{ij}$ if $\xi \in \Omega$. The kernels $U_{ij}(\xi,x)$ and $T_{ij}(\xi,x)$ are the two-point Kelvin fundamental solutions for displacements and tractions, respectively (Brebbia et al., 1984). $t_j(x)$ is the traction at the field point corresponding to the field displacement $u_j(x)$, while $t_j^p(x)$ is the traction particular solution corresponding to the displacement particular solution $u_j^p(x)$.

In order to obtain the particular solutions, $u_i^p(x)$ and $t_i^p(x)$, consider that the inertia term in Eq. (1) is approximated according to the following functions:

$$\rho\overleftrightarrow{u}_j(x) = \sum_{k=1}^{m} f(x,y_k)\alpha_j(y_k) \tag{3}$$

where $f(x, y_k)$ is chosen as any suitable function, $y_k (k = 1 \to m)$ are new field points, and $\alpha_j(y_k)$ are unknown coefficients related to the mentioned new field points. Substituting Eq. (3) into Eq. (1) with no boundary conditions yields:

$$Gu_{i,jj}^p(x) + \frac{G}{(1-2v)}u_{j,ji}^p(x) = \sum_{k=1}^{m} f(x,y_k)\alpha_j(y_k) \tag{4}$$

Representing the displacement particular solution, $u_i^p(x)$, by the following collocation scheme:

$$u_j^{\mathrm{p}}(x) = \sum_{k=1}^{m} \Psi_{jl}(x, y_k)\alpha_l(y_k) \tag{5}$$

where $\Psi_{jl}(x, y_k)$ is a displacement kernel between the field points x and y_k. And substituting Eq. (5) into Eq. (4), the relationship between $\Psi_{jl}(x, y_k)$ and $f(x, y_k)$ can be obtained as follows:

$$G\Psi_{ij,ll}(x, y_k) + \frac{G}{(1-2v)}\Psi_{il,lj}(x, y_k) = f(x, y_k)\delta_{ij} \tag{6}$$

Following a similar procedure, the traction particular solutions, $t_i^{\mathrm{p}}(x)$, is presented by the following collocation scheme:

$$t_j^{p}(x) = \sum_{k=1}^{m} \eta_{jl}(x, y_k)\alpha_l(y_k) \tag{7}$$

where $\eta_{jl}(x, y_k)$ is a traction kernel between the field points x and y_k, and could be derived from the displacement kernel, $\Psi_{jl}(x, y_k)$ as follows (Rashed, 2002a):

$$\eta_{ij}(x, y_k) = G\left[\frac{2v}{(1-2v)}\delta_{il}\Psi_{j\beta,\beta}(x, y_k) + \Psi_{ji,l}(x, y_k) + \Psi_{jl,i}(x, y_k)\right]n_l(y_k) \tag{8}$$

where δ_{ij} is the unity matrix which equals zero when $i \neq j$ and equals one when $i = j$, and n_l is the component of the outward surface normal at the field point y_k. Substituting Eqs. (5) and (7) into Eq. (2) and recall Eq. (3), the final integral form can be obtained as follows:

$$\begin{aligned} c_{ij}(\xi)u_j(\xi) + \int_{\Gamma_{(X)}} T_{ij}(\xi, x)u_j(x)\,\mathrm{d}\Gamma(x) = {} & \int_{\Gamma_{(X)}} U_{ij}(\xi, x)t_j(x)\,\mathrm{d}\Gamma(x) \\ & + \sum_{k=1}^{m}\left[c_{ij}(\xi)\Psi_{jl}(\xi, y_k) + \int_{\Gamma_{(X)}} T_{ij}(\xi, x)\Psi_{jl}(x, y_k)\,\mathrm{d}\Gamma(x)\right. \\ & \left. - \int_{\Gamma_{(X)}} U_{ij}(\xi, x)\eta_{jl}(x, y_k)\,\mathrm{d}\Gamma(x)\right] \times \rho\sum_{k=1}^{m} f^{-1}(x, y_k)\overleftrightarrow{u} \end{aligned} \tag{9}$$

Eq. (9) is used in the analysis. However, the expressions for $\Psi_{jl}(x, y_k)$, and $\eta_{jl}(x, y_k)$ have to be developed first.

3. Multiquadric approximation function and the corresponding Ψ_{jl} and η_{jl}

The function f in Eq. (3) is selected in this paper to be the multiquadric radial basis function (MQ), i.e.:

$$f = f(x, y_k) = \sqrt{R^2 + C^2} \tag{10}$$

where $R = R(x, y_k)$ is the Euclidian distance between the two field points x and y_k as shown in Fig. 1, and C is an arbitrary constant defined as the shape parameter (Golberg et al., 1996). In order to obtain the corresponding particular solution kernels of the MQ function, $\Psi_{ij}(x, y_k)$ and $\eta_{ij}(x, y_k)$, the following procedure is proposed: consider that the displacement kernel $\Psi_{ij}(x, y_k)$ is represented in terms of Galerkin vector components such as:

$$\Psi_{ij}(x, y_k) = V_{ij,mm}(x, y_k) - \frac{1}{2(1-v)}V_{im,jm}(x, y_k) \tag{11}$$

where the Galerkin vector $V_{ij}(x, y_k)$ can be evaluated according to the following equation:

$$V_{ij}(x, y_k) = \frac{1}{G}g(x, y_k)\delta_{ij} \tag{12}$$

in which the function $g(x, y_k)$ in the former equation is the particular solution of the following bi-harmonic equation:

$$\nabla^4 g(x,y_k) = f(x,y_k) = \sqrt{R^2+C^2} \tag{13}$$

where $\nabla^4 = \nabla^2\nabla^2$ is the 2D bi-harmonic operator. A suitable scalar particular solution of Eq. (13) can be obtained as follows:

$$g = \frac{(5R^2-2C^2)C^3}{60}\ln\left(\frac{R}{C+\sqrt{R^2+C^2}}\right) - \frac{C^3R^2}{12}\ln(C) + \frac{\sqrt{R^2+C^2}}{900}(4R^4+48R^2C^2-61C^4) \tag{14}$$

According to Eq. (12), the expressions of $V_{ij,mm}(x,y_k)$ and $V_{im,jm}(x,y_k)$ can be derived as follows:

$$\begin{aligned} V_{ij,mm} = \frac{\delta_{ij}}{G}\Bigg[&\frac{C^3}{3}\ln\left(\frac{R}{C(C+\sqrt{C^2+R^2})}\right) + \frac{20R^6+120R^4C^2+135R^2C^4+14C^6}{180(R^2+C^2)^{3/2}} \\ &- \frac{(25R^4+28R^2C^2-4C^4)C^3}{60(R^2+C^2)^{3/2}(C+\sqrt{R^2+C^2})} + \frac{(5R^2-2C^2)C^3R^2}{60(R^2+C^2)(C+\sqrt{R^2+C^2})^2}\Bigg] \end{aligned} \tag{15}$$

$$\begin{aligned} V_{im,jm} = \frac{1}{G}\Bigg[&\left(\frac{C^3}{6}\ln\left(\frac{R}{C(C+\sqrt{C^2+R^2})}\right) + \frac{4R^6+36R^4C^2+39R^2C^4+7C^6}{180(R^2+C^2)^{3/2}}\right.\\ &\left. + \frac{(5R^2-2C^2)C^3}{60R^2} - \frac{(5R^4+3R^2C^2-2C^4)C^3}{60(R^2+C^2)^{3/2}(C+\sqrt{R^2+C^2})}\right)\delta_{ij} \\ &+ \left(\frac{(5R^2-2C^2)C^3R^2}{60(R^2+C^2)(C+\sqrt{R^2+C^2})^2} - \frac{(15R^2+22C^2)C^3R^2}{60(R^2+C^2)^{3/2}(C+\sqrt{R^2+C^2})}\right.\\ &\left. + \frac{(12R^4+48R^2C^2+57C^4)R^2}{180(R^2+C^2)^{3/2}} + \frac{(5R^2+2C^2)C^3}{30R^2}\right)R_{,i}R_{,j}\Bigg] \end{aligned} \tag{16}$$

Substituting from Eqs. (15) and (16) into Eq. (11), the final expression of Ψ_{ij} can be obtained as follows:

$$\begin{aligned} \Psi_{ij} = \frac{\delta_{ij}}{2(1-\nu)G}\Bigg[&\left(\frac{C^3}{6}\ln\left(\frac{R}{C(C+\sqrt{C^2+R^2})}\right) + \frac{(15R^2+2C^2)C^3}{60R^2}\right.\\ &\left. + \frac{16R^6+84R^4C^2+96R^2C^4+7C^6}{180(R^2+C^2)^{3/2}} - \frac{(20R^4+25R^2C^2-2C^4)C^3}{60(R^2+C^2)^{3/2}(C+\sqrt{R^2+C^2})}\right.\\ &\left. + \frac{(5R^2-2C^2)C^3R^2}{60(R^2+C^2)(C+\sqrt{R^2+C^2})^2}\right) + (1-2\nu)\left(\frac{C^3}{3}\ln\left(\frac{R}{C(C+\sqrt{C^2+R^2})}\right)\right.\\ &\left. + \frac{C^3}{3} + \frac{20R^6+120R^4C^2+135R^2C^4+14C^6}{180(R^2+C^2)^{3/2}} - \frac{(25R^4+28R^2C^2-4C^4)C^3}{60(R^2+C^2)^{3/2}(C+\sqrt{R^2+C^2})}\right.\\ &\left. + \frac{(5R^2-2C^2)C^3R^2}{60(R^2+C^2)(C+\sqrt{R^2+C^2})^2}\right)\Bigg] - \frac{R_{,i}R_{,j}}{2(1-\nu)G}\Bigg[\frac{(5R^2+2C^2)C^3}{30R^2}\\ &+ \frac{(12R^4+48R^2C^2+57C^4)R^2}{180(R^2+C^2)^{3/2}} - \frac{(15R^2+22C^2)C^3R^2}{60(R^2+C^2)^{3/2}(C+\sqrt{R^2+C^2})}\\ &+ \frac{(5R^2-2C^2)C^3R^2}{60(R^2+C^2)(C+\sqrt{R^2+C^2})^2}\Bigg] \end{aligned} \tag{17}$$

Substituting in Eq. (8), the final expression for η_{ij} can be obtained as follows (where the relevant derivatives of Ψ_{ij} are listed in Appendix A):

$$
\begin{aligned}
\eta_{ij} = (N_i R_{,j} + \delta_{ij} R_{,N}) \Bigg[& \frac{(5R^2 - 2C^2)C^3}{30R^3} + \frac{(10R^4 + 15R^2C^2 - 2C^4)C^3 R}{20(R^2 + C^2)^2 (C + \sqrt{R^2 + C^2})^2} \\
& + \frac{(28R^6 - 20R^4 + 152R^4C^2 - 144R^2C^2 + 75R^2C^4 + 61C^4 + 56C^6)R}{300(R^2 + C^2)^{5/2}} \\
& - \frac{(10R^4 + 25R^2C^2 + 22C^4)C^3 R}{20(R^2 + C^2)^{5/2}(C + \sqrt{R^2 + C^2})} - \frac{(5R^2 - 2C^2)C^3 R^3}{30(R^2 + C^2)^{3/2}(C + \sqrt{R^2 + C^2})^3} \\
& - \left(\frac{v}{1 - v}\right) \Bigg(\frac{(5R^2 + 2C^2)C^3}{30R^3} + \frac{(12R^4 + 48R^2C^2 + 57C^4)R}{180(R^2 + C^2)^{3/2}} \\
& - \frac{(15R^2 + 22C^2)C^3 R}{60(R^2 + C^2)^{3/2}(C + \sqrt{R^2 + C^2})} + \frac{(5R^2 - 2C^2)C^3 R}{60(R^2 + C^2)(C + \sqrt{R^2 + C^2})^2} \Bigg) \Bigg] \\
& + N_j R_{,i} \Bigg[\left(\frac{v}{1 - v}\right) \cdot \Bigg(\frac{(5R^2 - 2C^2)C^3}{30R^3} + \frac{(10R^4 + 15R^2C^2 - 2C^4)C^3 R}{20(R^2 + C^2)^2 (C + \sqrt{R^2 + C^2})^2} \\
& + \frac{(28R^6 - 20R^4 + 152R^4C^2 - 144R^2C^2 + 75R^2C^4 + 61C^4 + 56C^6)R}{300(R^2 + C^2)^{5/2}} \\
& - \frac{(10R^4 + 25R^2C^2 + 22C^4)C^3 R}{20(R^2 + C^2)^{5/2}(C + \sqrt{R^2 + C^2})} - \frac{(5R^2 - 2C^2)C^3 R^3}{30(R^2 + C^2)^{3/2}(C + \sqrt{R^2 + C^2})^3} \Bigg) \\
& - \frac{(5R^2 + 2C^2)C^3}{30R^3} - \frac{(12R^4 + 48R^2C^2 + 57C^4)R}{180(R^2 + C^2)^{3/2}} \\
& + \frac{(15R^2 + 22C^2)C^3 R}{60(R^2 + C^2)^{3/2}(C + \sqrt{R^2 + C^2})} - \frac{(5R^2 - 2C^2)C^3 R}{60(R^2 + C^2)(C + \sqrt{R^2 + C^2})^2} \Bigg] \\
& + R_{,i} R_{,j} R_{,N} \left(\frac{v}{1 - v}\right) \Bigg[\frac{(10R^2 - 8C^2)C^3}{30R^3} - \frac{(10R^4 + 15R^2C^2 - 2C^4)C^3 R}{20(R^2 + C^2)^2 (C + \sqrt{R^2 + C^2})^2} \\
& - \frac{(28R^6 - 20R^4 + 152R^4C^2 - 144R^2C^2 + 75R^2C^4 + 61C^4 + 56C^6)R}{300(R^2 + C^2)^{5/2}} \\
& + \frac{(10R^4 + 25R^2C^2 + 22C^4)C^3 R}{20(R^2 + C^2)^{5/2}(C + \sqrt{R^2 + C^2})} + \frac{(5R^2 - 2C^2)C^3 R^3}{30(R^2 + C^2)^{3/2}(C + \sqrt{R^2 + C^2})^3} \\
& + \frac{(12R^4 + 48R^2C^2 + 57C^4)R}{60(R^2 + C^2)^{3/2}} - \frac{(15R^2 + 22C^2)C^3 R}{20(R^2 + C^2)^{3/2}(C + \sqrt{R^2 + C^2})} \\
& + \frac{(5R^2 - 2C^2)C^3 R}{20(R^2 + C^2)(C + \sqrt{R^2 + C^2})^2} \Bigg]
\end{aligned}
\tag{18}
$$

It has to be noted that the above expressions for Ψ_{ij} and η_{ij} cannot be evaluated at $R = 0$ since they both contain singular terms. To overcome this problem, a developed procedure for eliminating these singular terms is proposed in the next section.

4. Suggested technique for singularity canceling

First, the singular terms that appeared in the expression of Ψ_{ij} are isolated. This can be done by decomposing Ψ_{ij} into two parts; $\Psi_{ij}^{\text{singular}}$ and $\Psi_{ij}^{\text{non-singular}}$, in which:

$$\Psi_{ij}^{\text{non-singular}} = \Psi_{ij} - \Psi_{ij}^{\text{singular}} \tag{19}$$

where $\Psi_{ij}^{\text{singular}}$ contains the singular terms of order (ln R) and $(1/R^2)$, and is given by:

$$\Psi_{ij}^{\text{singular}} = \frac{1}{2(1-v)G}\left[\frac{(3-4v)C^3\delta_{ij}}{6}(\ln R) + \frac{(\delta_{ij}-2R_{,i}R_{,j})C^5}{30}\left(\frac{1}{R^2}\right)\right] \tag{20}$$

The proposed canceling technique is based on the idea that: particular solutions are not unique; therefore, any chosen particular solution, which must satisfies the Navier equation (Eq. (6)), can be added to Ψ_{ij} to form a new set of particular solution. Thus, the new set of smoothed particular solution $\hat{\Psi}_{ij}$ is defined as follows:

$$\hat{\Psi}_{ij} = \Psi_{ij} + c_1\overline{U}_{ij} + c_2\nabla^2\overline{U}_{ij} \tag{21}$$

where c_1 and c_2 are arbitrary constants, and $\overline{U}_{ij}$ and $\nabla^2\overline{U}_{ij}$ are chosen particular solutions of order $(\ln R)$ and $(1/R^2)$, respectively. These solutions must satisfy Navier equations as follows:

$$G\overline{U}_{ij,ll} + \frac{G}{(1-2v)}\overline{U}_{il,lj} = 0 \tag{22}$$

and:

$$G\nabla^2\overline{U}_{ij,ll} + \frac{G}{(1-2v)}\nabla^2\overline{U}_{il,lj} = 0 \tag{23}$$

The solution $\overline{U}_{ij}$ is chosen to be the displacement fundamental solution in terms of R, which can be expressed by:

$$\overline{U}_{ij} = \frac{1}{8\pi G(1-v)}\left[-(3-4v)\delta_{ij}\ln R + R_{,i}R_{,j}\right] \tag{24}$$

and the corresponding Laplacian of $\overline{U}_{ij}$ can be obtained as follows:

$$\nabla^2\overline{U}_{ij} = \overline{U}_{ij,ll} = \frac{1}{8\pi G(1-v)R^2}\left[\delta_{ij} - 2R_{,i}R_{,j}\right] \tag{25}$$

Now, the constants c_1 and c_2 in Eq. (21) can be computed to cancel singular terms of the same order. This can be done by comparing different terms in Eqs. (24) and (25) with those in Eq. (20) to give:

$$c_1 = \frac{2\pi C^3}{3} \tag{26}$$

and

$$c_2 = -\frac{\pi C^5}{15} \tag{27}$$

It has to be noted that when $R = 0$, the new displacement kernel,$\hat{\Psi}_{ij}$ will not be singular since the singular parts of Ψ_{ij} (i.e. $\Psi_{ij}^{\text{singular}}$) are eliminated using the proposed superposition. Also the condition that $\hat{\Psi}_{ij}$ satisfies Navier's equation (Eq. (6)), is valid, in other words:

$$G\hat{\Psi}_{ij,ll} + \frac{G}{(1-2v)}\hat{\Psi}_{il,lj} = \sqrt{R^2+C^2}\delta_{ij} \tag{28}$$

is verified.

Similar to Ψ_{ij}, the same technique is used to cancel the singular terms in the traction kernel η_{ij} (Eq. (18)): consider η_{ij} is divided into two parts as follows:

$$\eta_{ij}^{\text{non-singular}} = \eta_{ij} - \eta_{ij}^{\text{singular}} \tag{29}$$

where $\eta_{ij}^{\text{singular}}$ contains terms of order $(1/R)$ and $(1/R^3)$ as follows:

$$\begin{aligned}\eta_{ij}^{\text{singular}} = {} & \frac{N_iR_{,j}}{1-v}\left[\frac{(2v-1)C^3}{6}\left(\frac{1}{R}\right) - \frac{C^5}{15}\left(\frac{1}{R^3}\right)\right] + \frac{N_jR_{,i}}{1-v}\left[\frac{(1-2v)C^3}{6}\left(\frac{1}{R}\right) - \frac{C^5}{15}\left(\frac{1}{R^3}\right)\right] \\ & + \frac{\delta_{ij}R_{,N}}{1-v}\left[\frac{(1-2v)C^3}{6}\left(\frac{1}{R}\right) - \frac{C^5}{15}\left(\frac{1}{R^3}\right)\right] - \frac{R_{,i}R_{,j}R_{,N}}{1-v}\left[-\frac{C^3}{3}\left(\frac{1}{R}\right) - \frac{4C^5}{15}\left(\frac{1}{R^3}\right)\right]\end{aligned} \tag{30}$$

The expression of the new smoothed traction kernel $\hat{\eta}_{ij}$ can be defined as follows:

$$\hat{\eta}_{ij} = \eta_{ij} + c_3\overline{T}_{ij} + c_4\nabla^2\overline{T}_{ij} \tag{31}$$

where c_3 and c_4 are arbitrary constants that will be chosen to cancel all singular terms. $\overline{T}_{ij}$ is a suitable traction fundamental solution corresponding to the $\overline{U}_{ij}$ field, which can be derived from Eq. (8) as follows:

$$\overline{T}_{ij} = -\frac{1}{4\pi(1-\nu)R}\left[((1-2\nu)\delta_{ij} + 2R_{,i}R_{,j})R_{,n} + (1-2\nu)(N_jR_{,i} - N_iR_{,j})\right] \tag{32}$$

It can be seen from Eq. (32) that $\overline{T}_{ij}$ contains terms of order $(1/R)$ which will be used in canceling similar terms in Eq. (30). $\nabla^2\overline{T}_{ij}$ is the Laplacian of $\overline{T}_{ij}$ which is equal to:

$$\nabla^2\overline{T}_{ij} = \overline{T}_{ij,ll} = -\frac{1}{4\pi(1-\nu)R^3}\left[N_iR_{,j} + N_jR_{,i} + \delta_{ij}R_{,n} - 4R_{,i}R_{,j}R_{,n}\right] \tag{33}$$

It can be also seen that $\nabla^2\overline{T}_{ij}$ contains terms of order $(1/R^3)$ which will be used in canceling similar terms in Eq. (30). It is easy to show that choosing $c_3 = c_1$ and $c_4 = c_2$ will cancel all singularities in $\hat{\eta}_{ij}$. Alternatively, the expression for $\hat{\eta}_{ij}$ can be directly obtained from $\hat{\Psi}_{ij}$ using Eq. (8). The new smoothed kernels $\hat{\Psi}_{ij}$ and $\hat{\eta}_{ij}$ will be used instead of Ψ_{ij} and η_{ij} in the general dynamic integral equation presented in Eq. (9).

5. Limiting case

In the collocation process, it is very important to compute the values of $\hat{\Psi}_{ij}$and $\hat{\eta}_{ij}$ when $R \to 0$, this can be obtained as follows:

$$\lim_{R\to 0}\hat{\Psi}_{ij} = \frac{C^3}{72(1-\nu)G}[(27-32\nu) + (24\nu-18)\ln(2C^2)]\delta_{ij} \tag{34}$$

and:

$$\lim_{R\to 0}\hat{\eta}_{ij} = 0 \tag{35}$$

6. Boundary elements modeling

The boundary integral equation in Eq. (9) can be solved numerically by discretizing the boundary into elements. Quadratic shape functions are used along any element to represent its displacements and tractions. For any collocating source point, ξ_i, Eq. (9) can be rewritten as follows (Brebbia et al., 1984):

$$\begin{aligned}\sum_{j=1}^{N}[\mathbf{H}(\xi_i,\mathbf{x}_j)]_{2N\times 2N}[\mathbf{u}(\mathbf{x}_j)]_{2N\times 1} = {} & \sum_{j=1}^{N}[\mathbf{G}(\xi_i,\mathbf{x}_j)]_{2N\times 6NE}[\mathbf{t}(\mathbf{x}_j)]_{6NE\times 1} \\ & + \sum_{k=1}^{m}\left[\sum_{j=1}^{N}[\mathbf{H}(\xi_i,\mathbf{x}_j)]_{2N\times 2N}[\widehat{\mathbf{\Psi}}(\mathbf{x}_j,\mathbf{y}_k)]_{2N\times 2N}\right. \\ & \left. - \sum_{j=1}^{N}[\mathbf{G}(\xi_i,\mathbf{x}_j)]_{2N\times 6NE}[\widehat{\boldsymbol{\eta}}(\mathbf{x}_j,\mathbf{y}_k)]_{6NE\times 2N}\right] \\ & \times \rho\sum_{j=1}^{N}[\mathbf{F}^{-1}(\mathbf{y}_k,\mathbf{x}_j)]_{2N\times 2N}[\ddot{\mathbf{u}}(\mathbf{x}_j)]_{2N\times 1}\end{aligned} \tag{36}$$

where [**H**] and [**G**] are the well-known boundary element influence matrices. [**u**] and [**t**] are the vectors of boundary displacements and tractions, respectively, and N and NE are the number of boundary nodes and elements, respectively. $[\Psi]$ and $[\widehat{\eta}]$ are the matrices of displacement and traction particular solutions according to Eqs. (21) and (31). [**F**] is a collocation matrix based on the MQ function (Eq. (10)) and [ü] is the acceleration vector. The vector of collocation points $\mathbf{x}_j$, represent the N number of boundary nodes, whereas the other collocation scheme $\mathbf{y}_j$, represent m number of field points which will be chosen to be equal to N $(m = N)$ to obtain square matrix. Eq. (36) can be written in compact form as follows:

$$[\mathbf{H}][\mathbf{u}] = [\mathbf{G}][\mathbf{t}] + [\mathbf{M}][\ddot{\mathbf{u}}] \tag{37}$$

where [**M**] is mass matrix. It has to be noted that in Eq. (37) both the displacement and traction vectors are defined at a certain time t, i.e. $[\mathbf{u}] = [\mathbf{u}]_t$ and $[\mathbf{t}] = [\mathbf{t}]_t$. The acceleration in this equation [ü] will be expressed in terms of [**u**] according to the following Houbolt finite difference scheme (Bathe, 1982):

$$[\ddot{\mathbf{u}}]_{t+\Delta t} = \frac{2[\mathbf{u}]_{t+\Delta t} - 5[\mathbf{u}]_t + 4[\mathbf{u}]_{t-\Delta t} - [\mathbf{u}]_{t-2\Delta t}}{\Delta t^2} \tag{38}$$

where Δt is the time step. Substituting Eq. (38) into Eq. (37), gives:

$$\left[\frac{2}{\Delta t^2}[\mathbf{M}] + [\mathbf{H}]\right][\mathbf{u}]_{t+\Delta t} = [\mathbf{G}][\mathbf{t}]_{t+\Delta t} - \frac{1}{\Delta t^2}[\mathbf{M}][5[\mathbf{u}]_t - 4[\mathbf{u}]_{t-\Delta t} + [\mathbf{u}]_{t-2\Delta t}] \tag{39}$$

where the former equation is solved for the unknown boundary displacements and tractions at time $t + \Delta t$.

7. Applications

In order to illustrate the validity and efficiency of the proposed MQ formulation, four different examples are studied. The numerical integrations are carried out using four Gauss points. The results are compared to other published results based on different approaches. The effect of the shape parameter value on the result accuracy is investigated. Finally, the last application results are obtained and graphed within a long time zone to examine the proposed interpolation stability. Internal points can be used to improve the accuracy (for details, see Dominguez, 1993).

7.1. Infinite strip under tension

The first example is the infinite rectangular strip with the boundary conditions shown in Fig. 2. The strip dimensions are: 2 m wide and 4 m height, and is subjected to a Heaviside tension step load. The material properties of the strip are: $v = 0.25$, $G = 4 \times 10^4$ Pa, and $\rho = 1$ kg/m^3. The boundary is discretized into 12 elements and the time step Δt is taken to be 7.22×10^{-4} s. to allow the comparison of results with those obtained by Dominguez (1993) for the both $(1 + R)$ function and the analytical results (based on 1D solution). Fig. 3 demonstrates the displacement history at point "A" for different values of C (0.01 and 1.0). Results for other values for C between 0.01 and 1.0 are studied and showed behavior between the chosen values of C. Therefore, only results for $C = 0.01$ and $C = 1.0$ are plotted in Fig. 3. The results of Dominguez (1993) are also plotted on the same graph. It can be seen from the results that taking $C = 0.01$ gives the required efficient and stable results for the MQ function interpolation, therefore the value for $C = 0.01$ will be used in the next examples. This conclusion can be confirmed when studying the normal traction history at point "B" shown in Fig. 4. Finally, it can be seen that the MQ results are in excellent agreement with the analytical solution as much as the $(1 + R)$ results.

7.2. Simply supported deep beam

In this example, the simply supported deep beam with span length $L = 24$ and height $h = 6$ (shown in Fig. 5) is considered. The beam is subjected to a Heaviside uniform load with initial value $w = 0.01$, and its

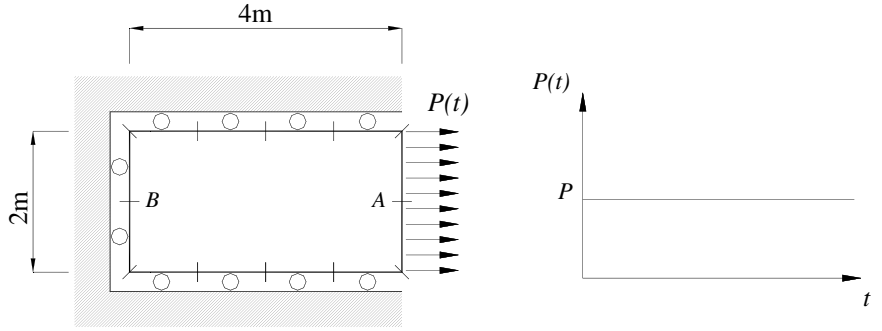

Fig. 2. Infinite strip under tension example.

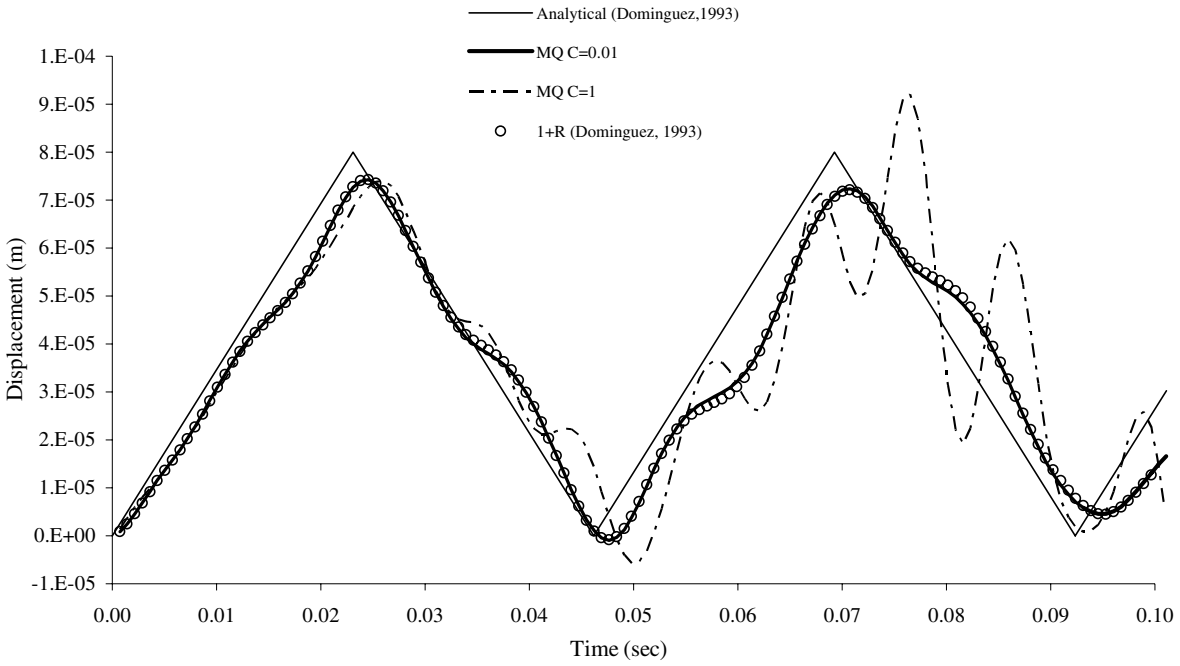

Fig. 3. Dynamic horizontal displacement of point "A" in the infinite strip example.

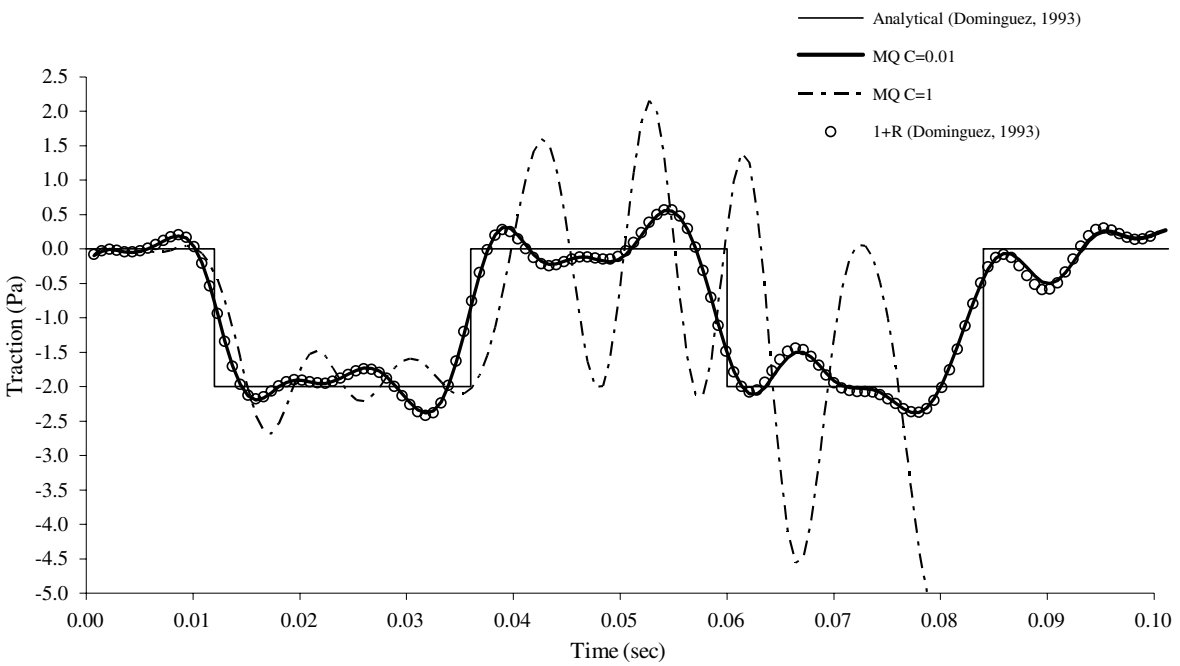

Fig. 4. Dynamic normal traction of point "B" in the infinite strip example.

material properties are: $v = 0.333$, $E = 100$, and $\rho = 1.5$. This problem was solved previously by Kontoni and Beskos (1993) using the conical $(1 + R)$ function. Due to symmetry, one half of the beam is analyzed using 24 boundary elements and restrained using the boundary conditions shown in Fig. 5. The results for the vertical displacement history at point "A" (located on the middle of the beam center line) using the MQ function ($C = 0.01$) are graphed in Fig. 6. The results obtained by Kontoni and Beskos (1993) for the same point using

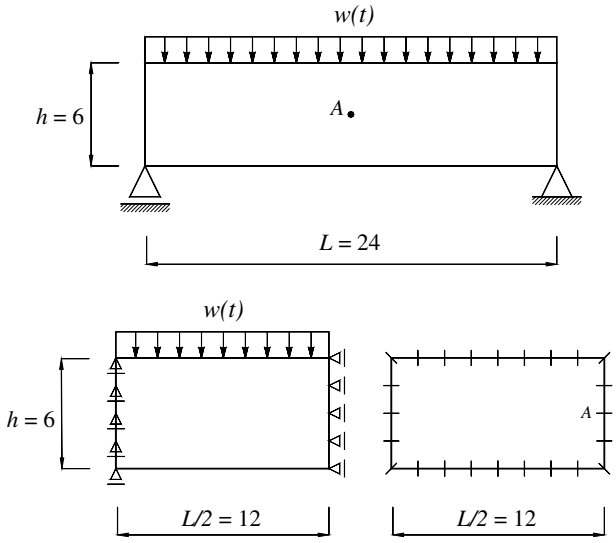

Fig. 5. The simply supported deep beam example.

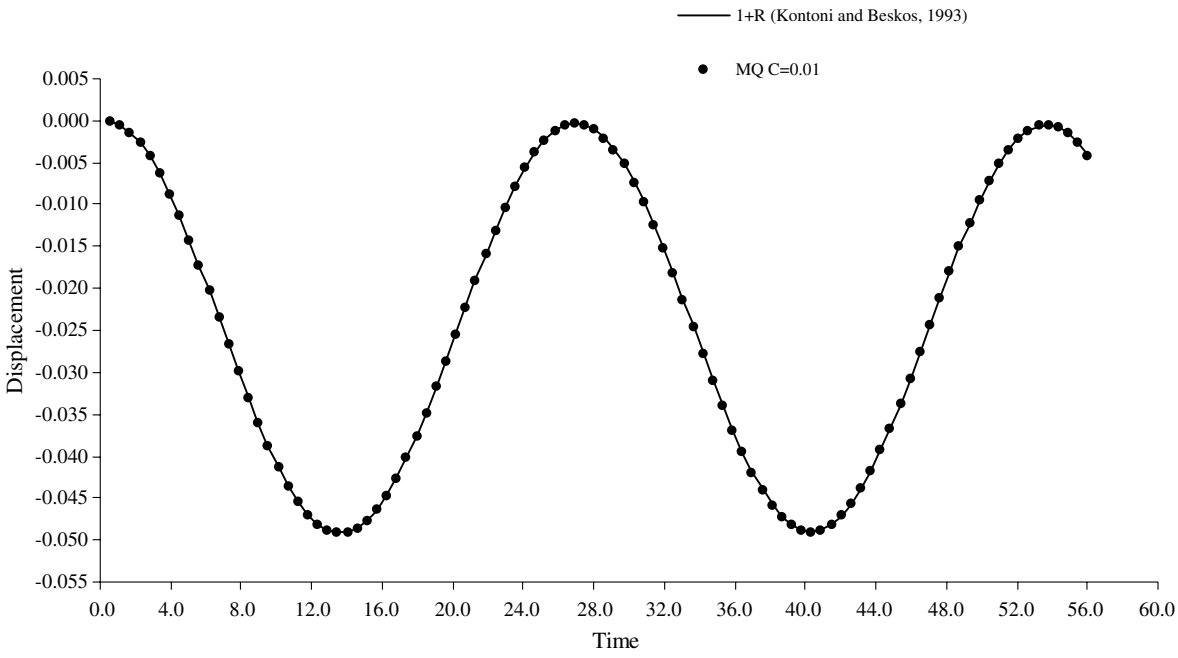

Fig. 6. Dynamic vertical displacement of point "A" in the deep beam example.

the $(1 + R)$ function are also plotted in the same graph. The results are almost identical which proofs the validity of the present formulation.viside tension load with initial value $P = 7500\ \mathrm{N/cm^2}$. The material properties are: $v = 0.3$, $E = 2.1 \times 10^7\ \mathrm{N/cm^2}$, and $\rho = 0.00785\ \mathrm{kg/m^3}$, and the time step Δt is taken to be 4×10^{-6} s. As it can be seen from Fig. 7, that one-quarter of the symmetric plate is considered with the shown boundary conditions. The boundary is discretized into 37 elements and 136 additional internal nodes are used to improve the result accuracy as shown in Fig. 7. The results for the displacement history of point "A" obtained using the MQ function ($C = 0.01$) is plotted in Fig. 8 and the results obtained by Agnantiaris et al. (1996) for the same point using the $(1 + R)$ function are also plotted on the same graph. As it can be seen from Fig. 8 that the results of the MQ function are in excellent agreement with those of the $(1 + R)$ function.

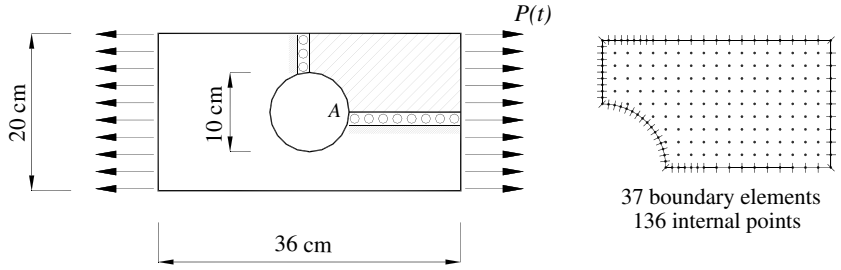

Fig. 7. The gusset plate example.

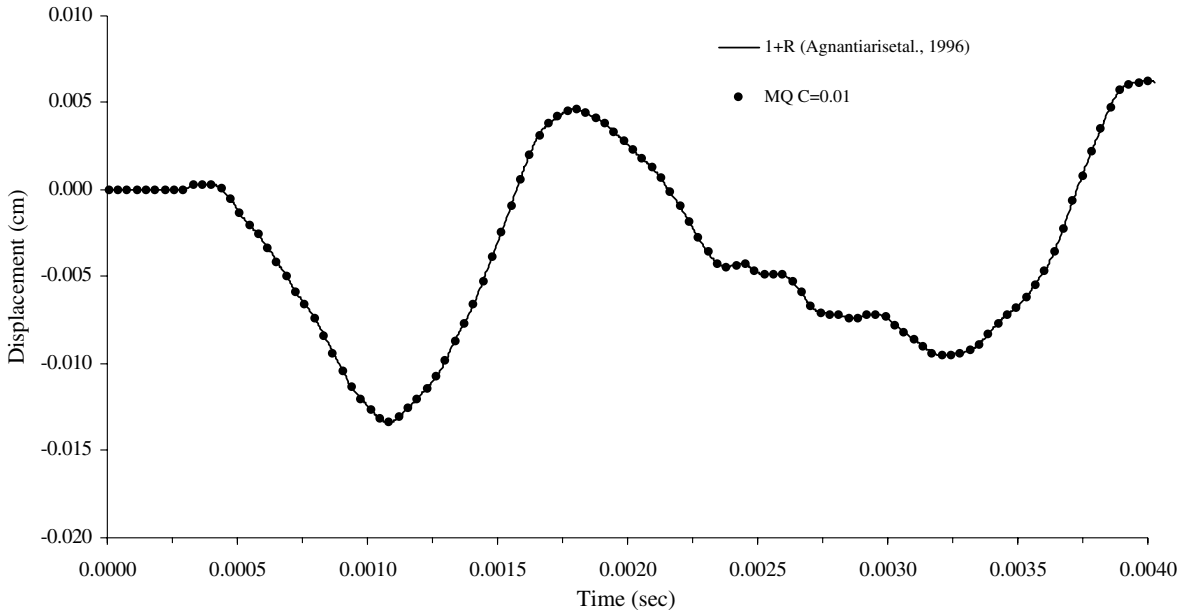

Fig. 8. Dynamic displacement of point "A" in the gusset plate example.

7.3. Interpolation function performance study

The validity of the present formulation is confirmed for different problems as presented in the previous examples. The purpose of this example is to demonstrate the superiority of the proposed formulation against the traditional $(1 + R)$ function. A comparison between the results obtained for the first example (infinite strip under tension) using MQ and $(1 + R)$ function are set up in the long time zone. The $(1 + R)$ function is chosen to be compared to as it gives the best accuracy among other functions, according to the conclusion of Agnantiaris et al. (1996). It is easy to observe that both function results match each other at early times ($t = 0$ to $t = 0.1$ s, as can be seen from Figs. 3 and 4). Therefore, this example focused on the behavior of these functions in the far time zone ($t = 1.3$ to $t = 1.8$ s. for displacement results, and $t = 0.4$ to $t = 0.85$ s. for traction results). The results of this study are shown in Figs. 9 and 10 for the displacement at point "A" and for the traction at point "B", respectively. It can be seen from these figures that the $(1 + R)$ function (as most of other functions) fails to give good interpolation scheme (oscillates) in the far time zone, whereas the interpolation using MQ function with $C = 0.01$ gives accurate and stable results along the whole studied time zone.

8. Conclusions

In this paper, a new formulation for the transient analysis of 2D elastodynamics is introduced. The DRM was successfully implemented using the MQ function in the interpolation of the inertia terms. The relevant

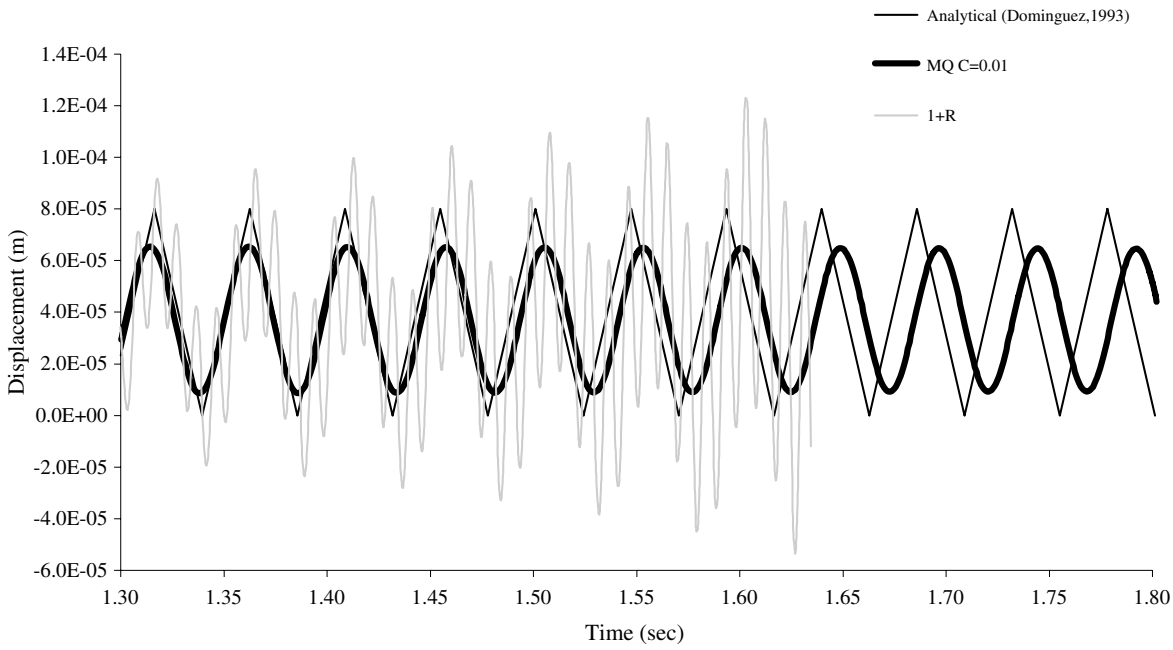

Fig. 9. Long time horizontal displacement of point "A" in the infinite strip example.

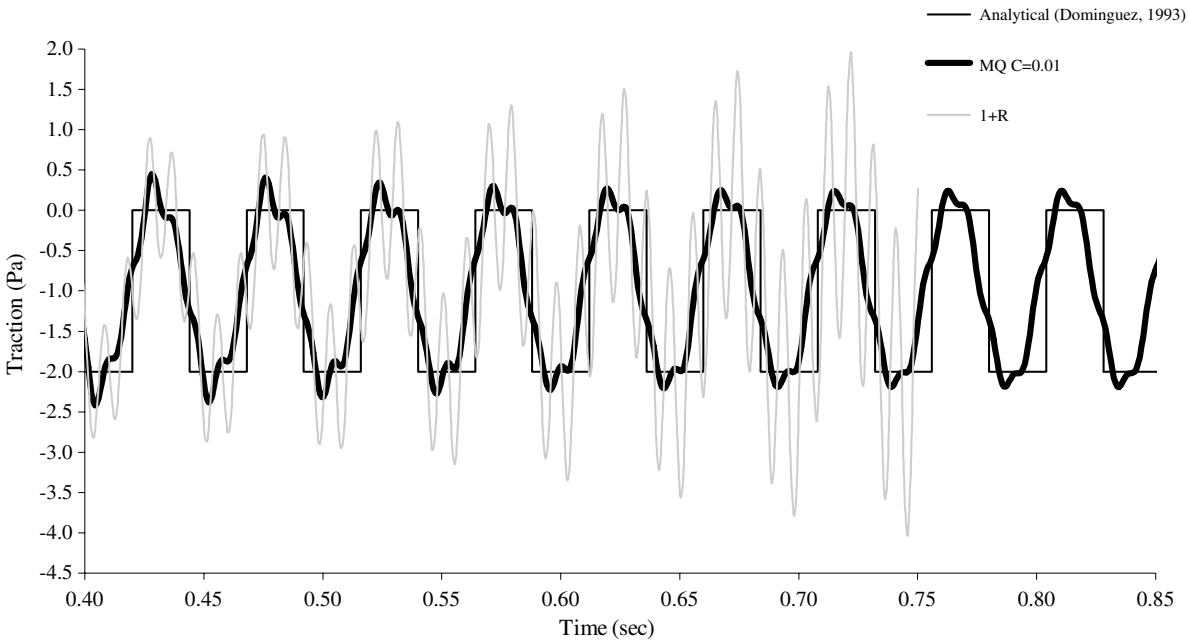

Fig. 10. Long time normal traction of point "B" in the infinite strip example.

expressions for displacement and traction particular solutions were derived, and then the singularities in the final expressions were canceled using a developed technique. The new formulation was examined throughout different applications and showed excellent performance. The results demonstrated that the MQ function is quite suitable for modeling different problems including stress concentration cases. Moreover, when the results of MQ function is being compared with those of the traditional $(1 + R)$ function in long time zone, the MQ function succeeded to give more stable and more accurate results. This leads to the conclusion that: the MQ function, as previously confirmed for surface generations from scattered data (Franke, 1982) and for potential

problems (Golberg et al., 1996), is the best radial basis function in modeling 2D structures under transient loading. Finally, although the choosing of the MQ shape parameter, C, to be equal to 0.01 seems to give enough accuracy in the studied applications, a future procedure such as the cross validation (see Golberg et al., 1996) has to be carried out to determine the best selection of its value.

Appendix A

The expressions of the Ψ_{ij} derivatives are:

$$\begin{aligned}
\Psi_{j\beta,\beta} = {} & \frac{(1-2\nu)R_{,j}}{2(1-\nu)G}\left[\left(\frac{C^3}{3}+\frac{(12R^4+48R^2C^2+57C^4)R}{180(R^2+C^2)^{3/2}}\right.\right.\\
& +\frac{(28R^6-20R^4+152R^4C^2-144R^2C^2+75R^2C^4+61C^4+56C^6)R}{300(R^2+C^2)^{5/2}}\\
& +\frac{(10R^4+25R^2C^2+22C^4)C^3R}{20(R^2+C^2)^{5/2}(C+\sqrt{R^2+C^2})}-\frac{(5R^2-2C^2)C^3R^3}{30(R^2+C^2)^{3/2}(C+\sqrt{R^2+C^2})^3}\\
& -\frac{(15R^2+22C^2)C^3R}{60(R^2+C^2)^{3/2}(C+\sqrt{R^2+C^2})}-\frac{(10R^4+25R^2C^2+22C^4)C^3R}{20(R^2+C^2)^2(C+\sqrt{R^2+C^2})^2}\\
& \left.\left.+\frac{(5R^2-2C^2)C^3R}{60(R^2+C^2)(C+\sqrt{R^2+C^2})^2}\right)\right]\\
\Psi_{ji,l} = {} & \frac{\delta_{ij}R_{,l}}{G}\left[\left(\frac{(5R^2-2C^2)C^3}{30R^3}+\frac{(10R^4+15R^2C^2-2C^4)C^3R}{20(R^2+C^2)^2(C+\sqrt{R^2+C^2})^2}\right.\right.\\
& +\frac{(28R^6-20R^4+152R^4C^2-144R^2C^2+75R^2C^4+61C^4+56C^6)R}{300(R^2+C^2)^{5/2}}\\
& \left.-\frac{(10R^4+25R^2C^2+22C^4)C^3R}{20(R^2+C^2)^{5/2}(C+\sqrt{R^2+C^2})}-\frac{(5R^2-2C^2)C^3R^3}{30(R^2+C^2)^{3/2}(C+\sqrt{R^2+C^2})^3}\right)\\
& +\frac{(1-2\nu)}{2(1-\nu)}\left(\frac{(5R^2+2C^2)C^3}{30R^3}+\frac{(12R^4+48R^2C^2+57C^4)R}{180(R^2+C^2)^{3/2}}\right.\\
& \left.\left.-\frac{(15R^2+22C^2)C^3R}{60(R^2+C^2)^{3/2}(C+\sqrt{R^2+C^2})}+\frac{(5R^2-2C^2)C^3R}{60(R^2+C^2)(C+\sqrt{R^2+C^2})^2}\right)\right]\\
& -\frac{(\delta_{jl}R_{,i}+\delta_{il}R_{,j})}{2(1-\nu)G}\left[\left(\frac{(5R^2+2C^2)C^3}{30R^3}+\frac{(12R^4+48R^2C^2+57C^4)R}{180(R^2+C^2)^{3/2}}\right.\right.\\
& \left.\left.-\frac{(15R^2+22C^2)C^3R}{60(R^2+C^2)^{3/2}(C+\sqrt{R^2+C^2})}+\frac{(5R^2-2C^2)C^3R}{60(R^2+C^2)(C+\sqrt{R^2+C^2})^2}\right)\right]\\
& -\frac{R_{,i}R_{,j}R_{,l}}{2(1-\nu)G}\left[\frac{(-10R^2+4C^2)C^3}{30R^3}+\frac{(10R^4+15R^2C^2-2C^4)C^3R}{20(R^2+C^2)^2(C+\sqrt{R^2+C^2})^2}\right.\\
& +\frac{(28R^6-20R^4+152R^4C^2-144R^2C^2+75R^2C^4+61C^4+56C^6)R}{300(R^2+C^2)^{5/2}}\\
& -\frac{(10R^4+25R^2C^2+22C^4)C^3R}{20(R^2+C^2)^{5/2}(C+\sqrt{R^2+C^2})}-\frac{(5R^2-2C^2)C^3R^3}{30(R^2+C^2)^{3/2}(C+\sqrt{R^2+C^2})^3}\\
& -\frac{(12R^4+48R^2C^2+57C^4)R}{60(R^2+C^2)^{3/2}}+\frac{(15R^2+22C^2)C^3R}{20(R^2+C^2)^{3/2}(C+\sqrt{R^2+C^2})}\\
& \left.-\frac{(5R^2-2C^2)C^3R}{20(R^2+C^2)(C+\sqrt{R^2+C^2})^2}\right]
\end{aligned}$$

References

Agnantiaris, J.P., Polyzos, D., Beskos, D.E., 1996. Some studies on dual reciprocity BEM for elastodynamic analysis. Comput. Mech. (17), 270–277.

Agnantiaris, J.P., Polyzos, D., Beskos, D.E., 2001. Free vibration analysis of non-axisymmetric and axisymmetric structures by the dual reciprocity BEM. Eng. Anal. Bound. Elem. (25), 713–723.

Bathe, K.-J., 1982. Finite Element Procedure in Engineering Analysis. Prentice-Hall, Englewood Cliffs, NJ.

Brebbia, C.A., Telles, J.C.F., Wrobel, L.C., 1984. Boundary Element Techniques: Theory and Applications in Engineering. Springer-Verlag, Berlin.

Bridges, T.R., Wrobel, L.C., 1994. On the calculation of natural frequencies of microstructures using DRBEM. BEM XVI conference, Computational Mechanics Publications, Southampton, London.

Chen, C.S., 1995. The method of fundamental solutions for non-linear thermal explosions. Commun. Numer. Meth. Eng. (11), 675–681.

Coda, H.B., Venturini, W.S., 2000. Dynamic non-linear stress analysis by the mass matrix BEM. Eng. Anal. Bound. Elem. (24), 623–632.

Dominguez, J., 1993. Boundary Element in Dynamics. Computational Mechanics Publications/Elsevier Applied Science, Southampton/London.

Franke, R., 1982. Scattered data interpolation: tests of some methods. Math. Comput. (48), 181–200.

Golberg, M.A., Chen, C.S., 1994. The theory of radial basis functions applied to the BEM for inhomogeneous partial differential equations. Bound. Elem. Commun. (5), 57–61.

Golberg, M.A., 1995. The numerical evaluation of particular solutions in the BEM-a review. Bound. Elem. Commun. (6), 99–106.

Golberg, M.A., Chen, C.S., Karur, S.R., 1996. Improved multiquadric approximation for partial differential equations. Eng. Anal. Bound. Elem. (18), 9–17.

Hardy, R.L., 1971. Multiquadric equations of topography and other irregular surfaces. J. Geophy. Res. (176), 1905–1917.

Hardy, R.L., 1990. Theory and applications of the multiquadric–biharmonic method: 20 years of discovery. Comput. Math. App. 19 (8/9), 163–208.

Karur, S.R., Ramachandran, P.A., 1995. Augmented thin plate spline approximation in DRM. Bound. Elem. Commun. (6), 55–58.

Kontoni, D.P.N., Beskos, D.E., 1993. Transient dynamic elastoplastic analysis by the dual reciprocity BEM. Eng. Anal. Bound. Elem. (12), 1–16.

Madych, W.R., Nelson, S.A., 1992. Bounds on multivariate polynomials and exponential error estimates for multiquadric interpolation. J. Approx. Theory 70 (1), 94–114.

Nardini, D., Brebbia, C.A., 1982. A new approach to free vibration analysis using boundary elements. Proc. 4th Int. Conf. Boundary Elements., Computational Mechanics Publications, Southampton and Springer-Verlag, Berlin, pp. 313–326.

Niku, S.M., Adey, R.A., 1996. Computational aspect of the dual reciprocity method for dynamics Technical Note. Eng. Anal. Bound. Elem. (18), 43–61.

Partridge, P.W., Brebbia, C.A., Wrobel, L.C., 1992. The Dual Reciprocity Boundary Element Method. Computational Mechanics Publications/Elsevier Applied Science, Southampton/London.

Perez-Gavilan, J.J., Aliabadi, M.H., 2000. A Galerkin boundary element formulation with dual reciprocity for elastodynamics. Int. J. Numer. Meth. Eng. (48), 1331–1344.

Powell, M.J., 1994. The uniform convergence of thin plate spline interpolation in two dimensions. Numer. Math. 68 (1), 107–128.

Rashed, Y.F., 2002a. Transient dynamic boundary element analysis using Gaussian based mass matrix. Eng. Anal. Bound. Elem. (26), 265–279.

Rashed, Y.F., 2002b. BEM for dynamic analysis using compact supported radial basis functions. Comput. Struc. (80), 1351–1367.

Telles, J.C.F., Carrer, J.M.A., 1994. Static and transient dynamic non-linear stress analysis by the boundary element method with implicit techniques. Eng. Anal. Bound. Elem. (14), 65–74.

Wendland, H., 2002. Fast evaluation of radial basis functions: methods based on partition of unity. In: Chui, C.K., Schumaker, L.L., Stöckler, J. (Eds.), Approximation Theory X: Wavelets, Splines, and Applications. Vanderbilt University Press, pp. 473–483.